Electronic Supplementary Information

NiPt-MnO_x supported on N-doped porous carbon derived from metal-organic frameworks for highly efficient hydrogen generation from hydrazine

Bingquan Xia[a], Teng Liu[a], Wei Luo[a,b,c*], Gongzhen Cheng[a]

[a]College of Chemistry and Molecular Sciences, Wuhan University, Wuhan, Hubei 430072, P. R. China. Tel.: +86 2768752366. **E-mail address*: wluo@whu.edu.cn

[b]Key Laboratory of Advanced Energy Materials Chemistry (Ministry of Education), Nankai University, Tianjin 300071, P. R. China

[c]Suzhou Institute of Wuhan University, Suzhou, Jiangsu, 215123, P. R. China

Preparation of Graphene Oxide (GO)

GO was prepared by a modified Hummers method. Typically, a mixture of concentrated H_2SO_4/H_3PO_4 (360:40 mL) was added to a mixture of graphite flakes (3.0 g) and $KMnO_4$ (18.0 g). The reaction was then heated to 50 °C and stirred for 12 h. The reaction was cooled down to room temperature and poured onto ice with 30% H_2O_2 (3 mL). Excess H_2O_2 was dropped to the above solution until the solution turned yellow, which indicates the complete oxidation of graphite. The resulting product was obtained by centrifugation. The product was then washed by deionized water, 30% diluted hydrochloric acid and ethanol for many times and dried under vacuum at 25 °C.

Preparation of $(Ni_3Pt_7)_{0.5}$-$(MnOx)_{0.5}$ immobilized on other supports

For comparison, NiPt-MnOx with optimized composition of Ni, Pt and Mn were also immobilized on other supports, including GO, Al_2O_3, SiO_2, PVP, activate carbon (EC-300J).

Preparation of $(Ni_3Pt_7)_{0.5}$-$(MnOx)_{0.5}$ /NPC-900-2h

To investigate the influence of reaction time on the catalyst, the preparation of $(Ni_3Pt_7)_{0.5}$-$(MnO_x)_{0.5}$/NPC-900-2h was similar to the preparation of $(Ni_3Pt_7)_{0.5}$-$(MnO_x)_{0.5}$/NPC-900 except that the reaction time was prolonged to 2h after the addition of $NaBH_4$.

All the above catalysts were then tested for hydrogen evolution from hydrazine in alkaline solution.

Calculation methods:

The H_2 selectivity (X) and $TOF_{initial}$ can be calculated using equation below

$$X = (3\lambda - 1)/8 \quad [\lambda = n_{N_2+H_2} / n_{H_2NNH_2}]$$

$$TOF_{initial} = \frac{P_{atm} V_{N_2+H_2} / RT}{n_{Ni+Pt} t}$$

Where $TOF_{initial}$ is initial turnover frequency, P_{atm} is the atmospheric pressure, $V_{N_2+H_2}$ is the volume of the generated gas when the conversion reached 50%, *R* is the universal gas constant, *T* is room temperature (298 K), n_{Ni+Pt} is the mole amount of Ni and Pt, and *t* is the reaction time. (N.B. The TOF values were determined by considering only the active sites of Ni and Pt, when the conversion reached 50%.)

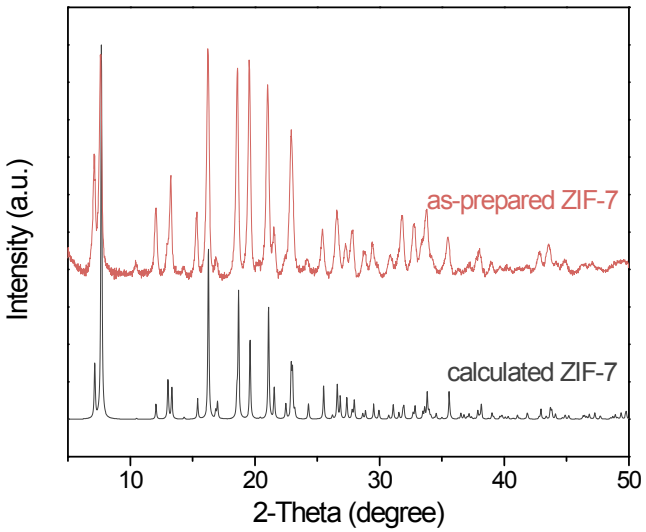

Figure S1. Powder XRD patterns of ZIF-7.

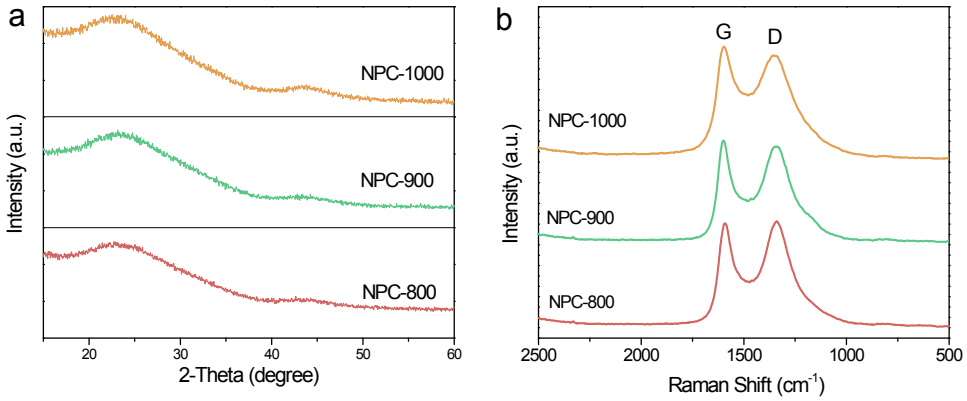

Figure S2. (a) Powder XRD patterns and (b) Raman spectra of ZIF-7 after calcination.

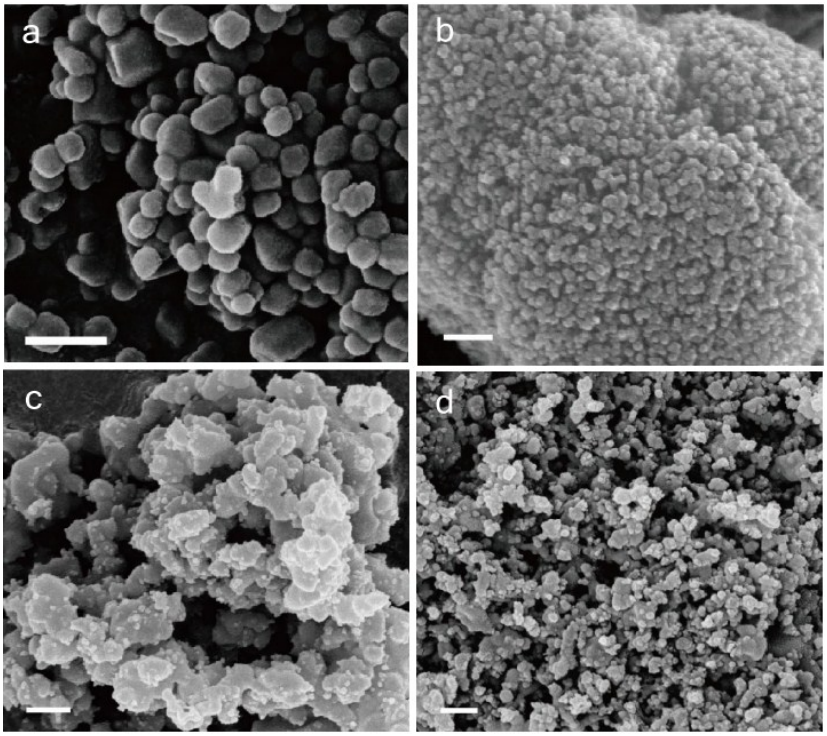

Figure S3. SEM images of (a) ZIF-7, (b) NPC-800, (b) NPC-900, (C) NPC-1000. (Scale bar = 200 nm)

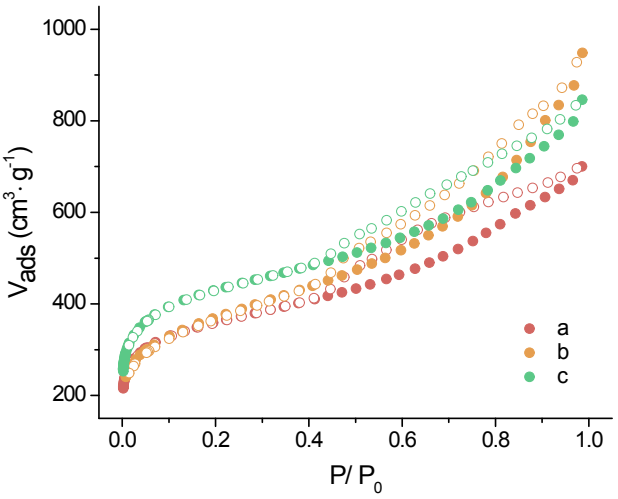

Figure S4. N_2 adsorption–desorption isotherms of (a) NPC-800, (b) NPC-900 and (c) NPC-1000.

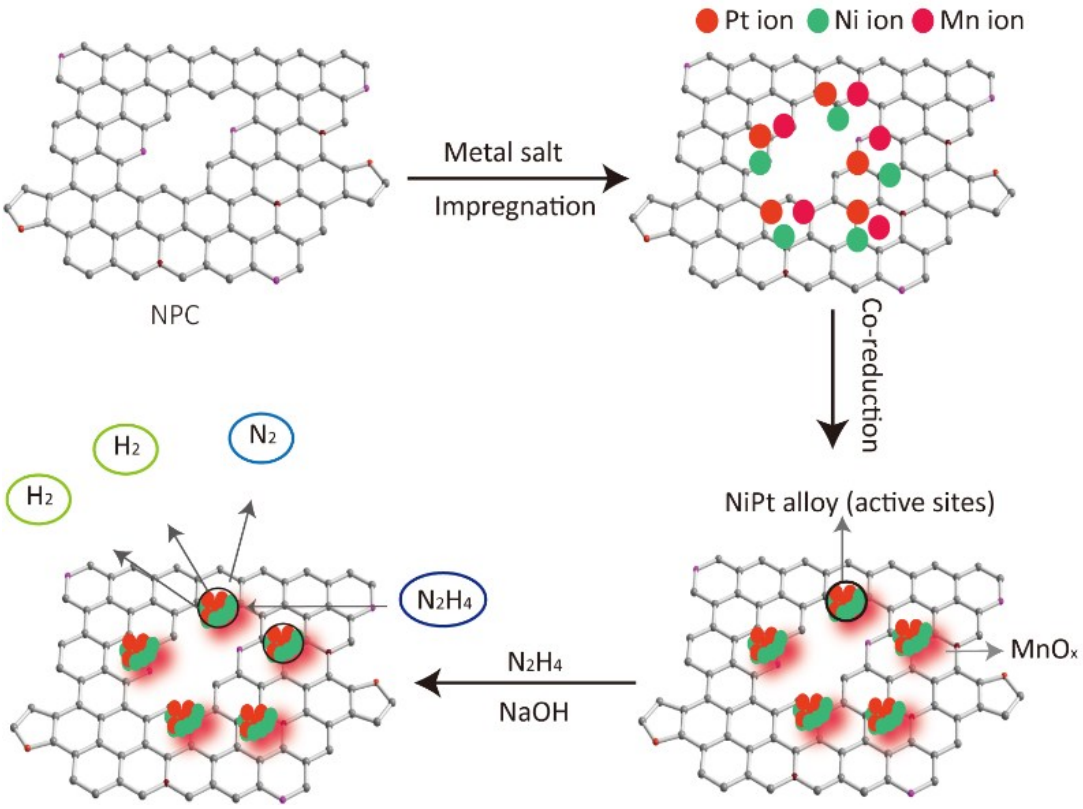

Figure S5. The schematic illustration of the immobilization of Pt, Ni and Mn on NPC derived from ZIF-7.

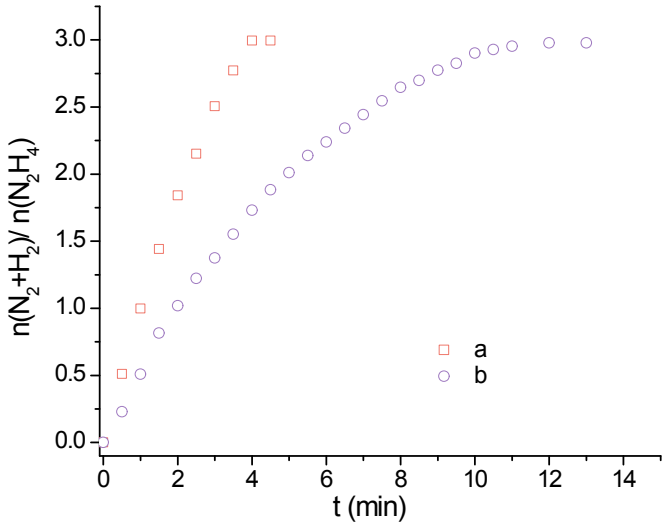

Figure S6. Catalytic performance tests of NiPt/NPC-900 with (a) and without (b) the addition of 0.1 mM Mn at 323 K.($n_{(Ni+Pt)}$ = 0.1 mmol)

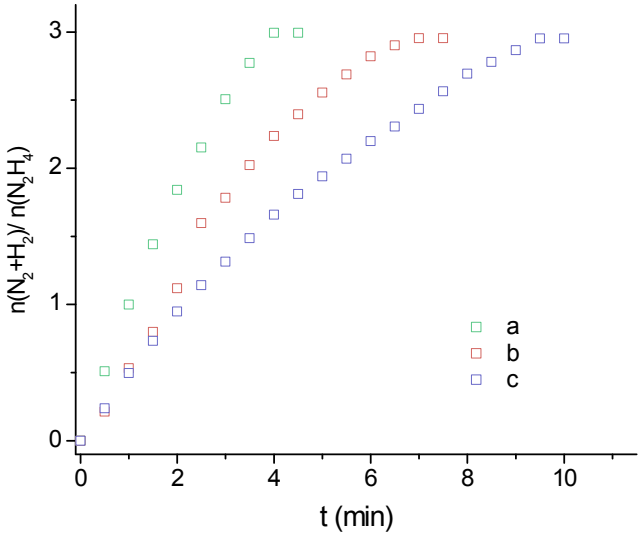

Figure S7. Catalytic performance tests of $(Ni_5Pt_5)_{0.5}$-$(MnO_x)_{0.5}$ stabilized on (a) NPC-900, (b) NPC-800, (c) NPC-1000 at 323 K. ($n_{(Ni+Pt+Mn)}$ = 0.2 mmol)

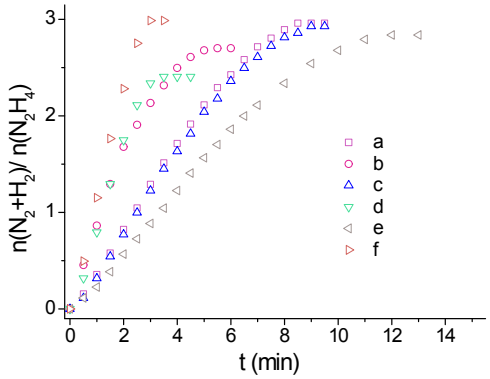

Figure S8. Catalytic performance tests of decomposition of hydrazine catalyzed by $(Ni_3Pt_7)_{0.5}$-$(MnO_x)_{0.5}$ stabilized on (a) RGO, (b) PVP, (c) Al_2O_3, (d) C-blcack (EC-300J), (e) SiO_2, (f) NPC-900 at 323 K. ($n_{(Ni+Pt+Mn)}$ = 0.2 mmol)

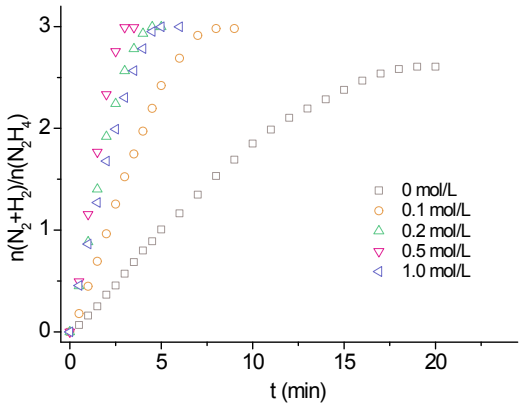

Figure S9. Catalytic performance tests of decomposition of hydrazine catalyzed by $(Ni_3Pt_7)_{0.5}$-$(MnO_x)_{0.5}$/NPC-900 in NaOH solution with different concentration at 323 K. ($n_{(Ni+Pt+Mn)}$ = 0.2 mmol)

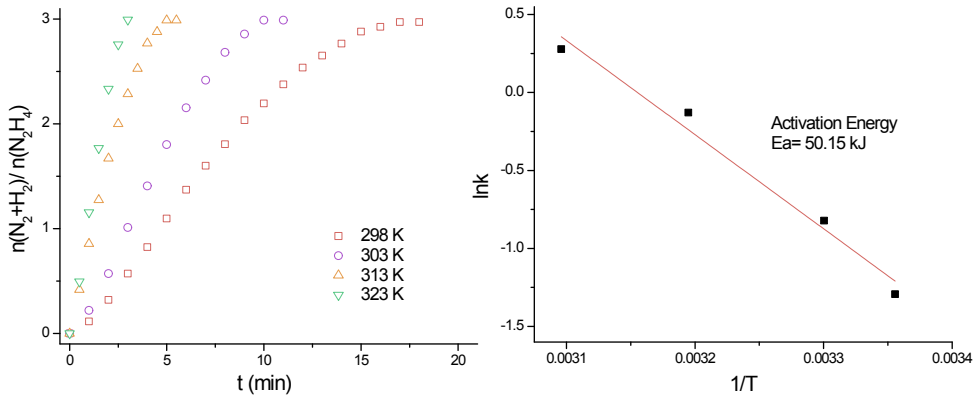

Figure S10. (a) Time course plots for hydrogen generation from the decomposition of hydrazine by $(Ni_3Pt_7)_{0.5}$-$(MnO_x)_{0.5}$/NPC-900 at 298 K, 303 K, 313 K and 323K. (b) Plot of ln k versus 1/T during the hydrazine decomposition over $(Ni_3Pt_7)_{0.5}$-$(MnO_x)_{0.5}$/ NPC-900 at different temperatures. ($n_{(Ni+Pt+Mn)}$ = 0.2 mmol)

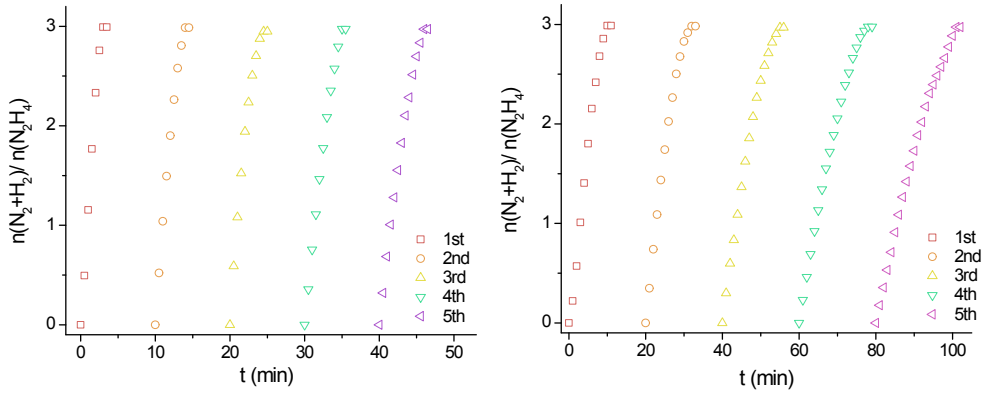

Figure S11. Durability tests of $(Ni_3Pt_7)_{0.5}$-$(MnO_x)_{0.5}$/NPC-900 on decomposition of hydrazine at (a) 323 K and (b) 303K. ($n_{(Ni+Pt+Mn)}$ = 0.2 mmol)

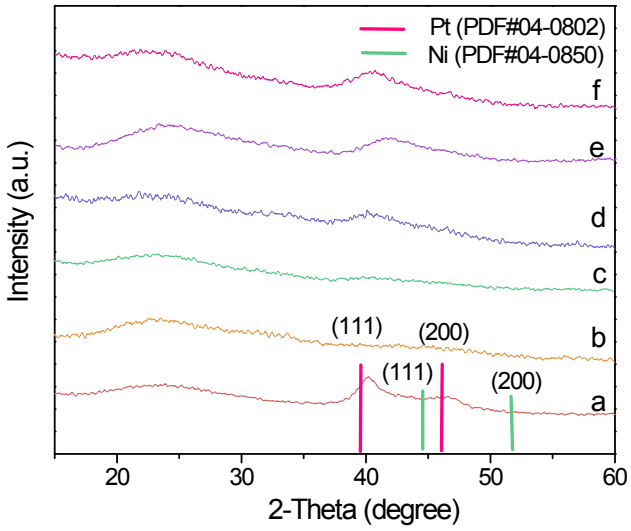

Figure S12. Powder XRD patterns for (a) Ni_3Pt_7/NPC-900, (b) $(Ni_9Pt_1)_{0.5}$-$(MnO_x)_{0.5}$/NPC-900, (c) $(Ni_7Pt_3)_{0.5}$-$(MnO_x)_{0.5}$/NPC-900, (d) $(Ni_5Pt_5)_{0.5}$-$(MnO_x)_{0.5}$/NPC-900, (e) $(Ni_3Pt_7)_{0.5}$-$(MnO_x)_{0.5}$/NPC-900 and (f) $(Ni_1Pt_9)_{0.5}$-$(MnO_x)_{0.5}$/NPC-900.

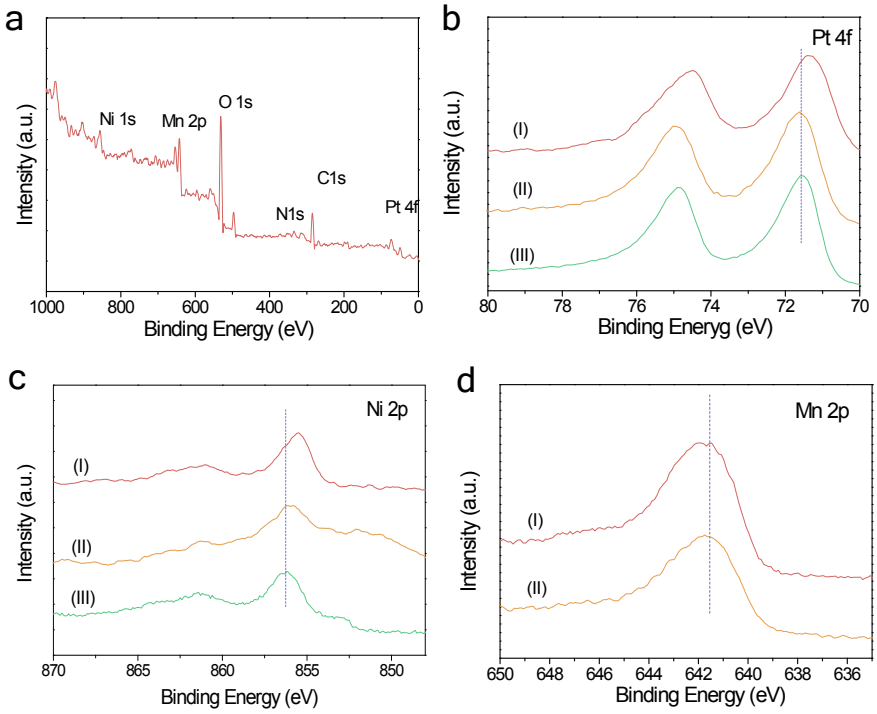

Figure S13. (a) XPS spectrum, (b) Pt 4f, (c) Ni 2p and (d) Mn 2p spectra for (I) $(Ni_3Pt_7)_{0.5}$-$(MnO_x)_{0.5}$/NPC-900, (II) $(Ni_3Pt_7)_{0.5}$-$(MnO_x)_{0.5}$ and (III)Ni_3Pt_7/NPC-900.

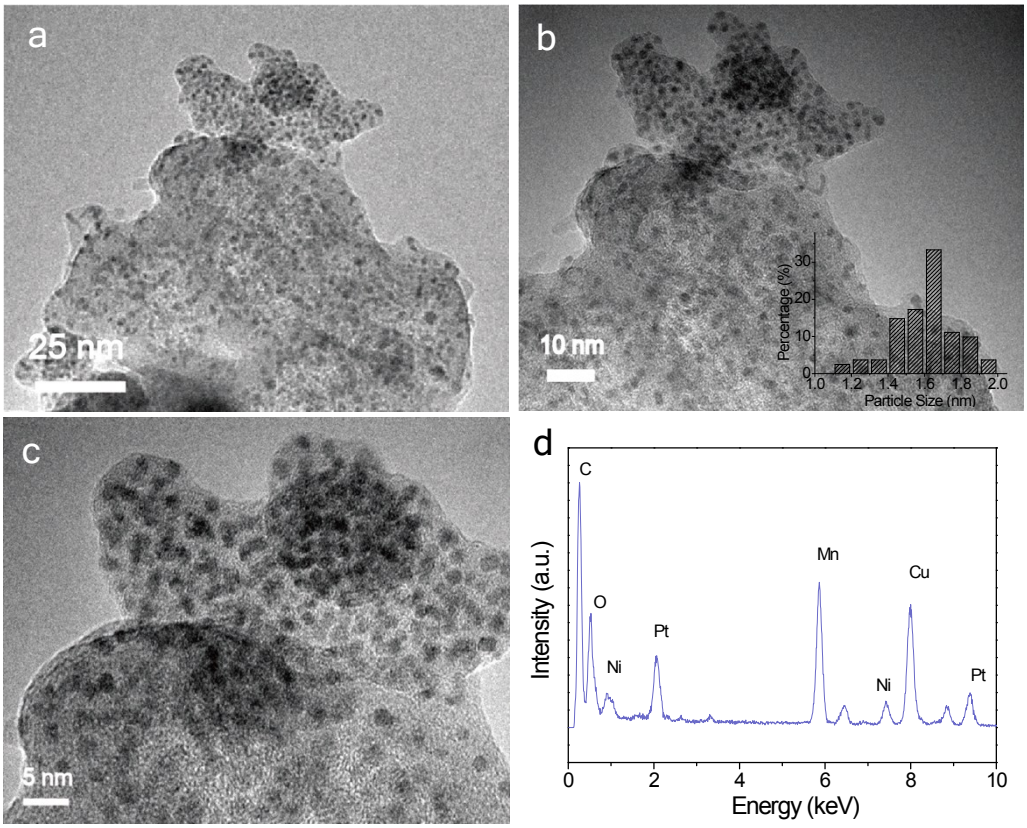

Figure S14. (a-c) TEM images of $(Ni_5Pt_5)_{0.5}$-$(MnO_x)_{0.5}$/NPC-900 with different magnifications, (b inset) corresponding particle size distribution and (d) EDX spectrum.

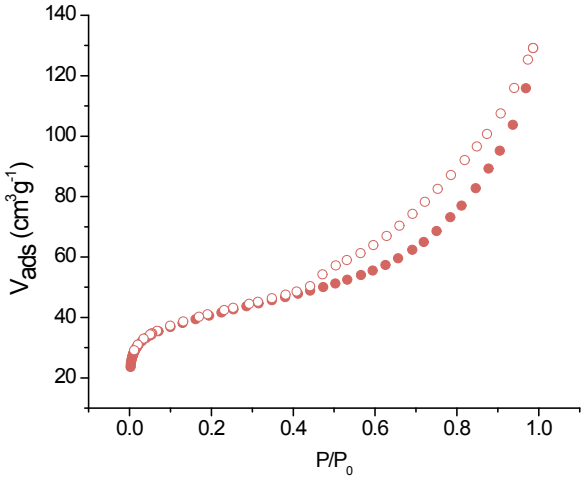

Figure S15. N_2 adsorption–desorption isotherms of $(Ni_3Pt_7)_{0.5}$-$(MnO_x)_{0.5}$/NPC-900.

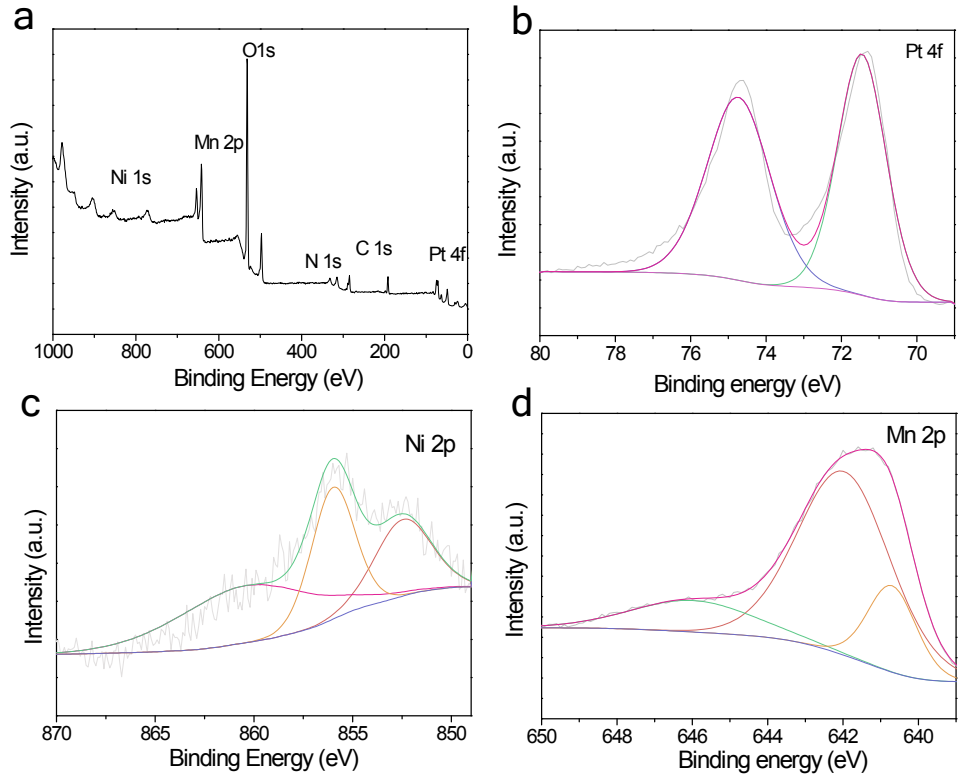

Figure S16. XPS spectrum for (a) $(Ni_3Pt_7)_{0.5}$-$(MnO_x)_{0.5}$/NPC-900-2h, and corresponding high resolution (b) Pt 4f, (c) Ni 2p and (d) Mn 2p spectrum.

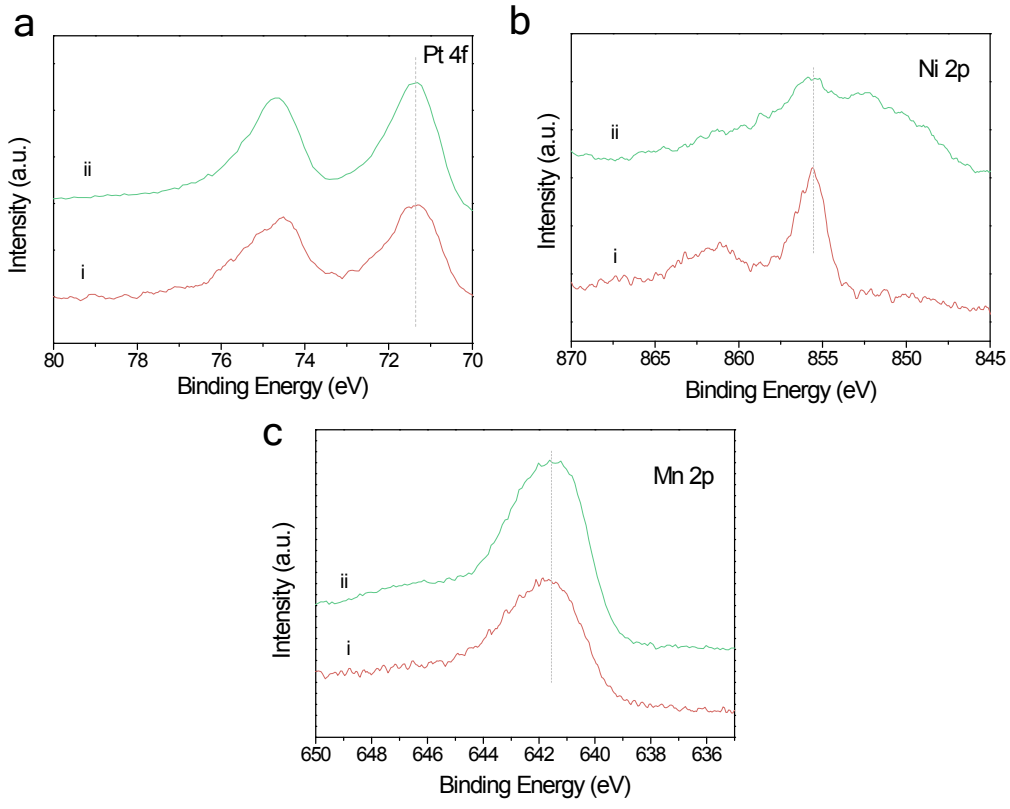

Figure S17. High resolution XPS spectra of (a) Pt 4f, (b) Ni 2p and (c) Mn 2p for (i) $(Ni_3Pt_7)_{0.5}$-$(MnO_x)_{0.5}$/NPC-900 and (ii) $(Ni_3Pt_7)_{0.5}$-$(MnO_x)_{0.5}$/NPC-900-2h.

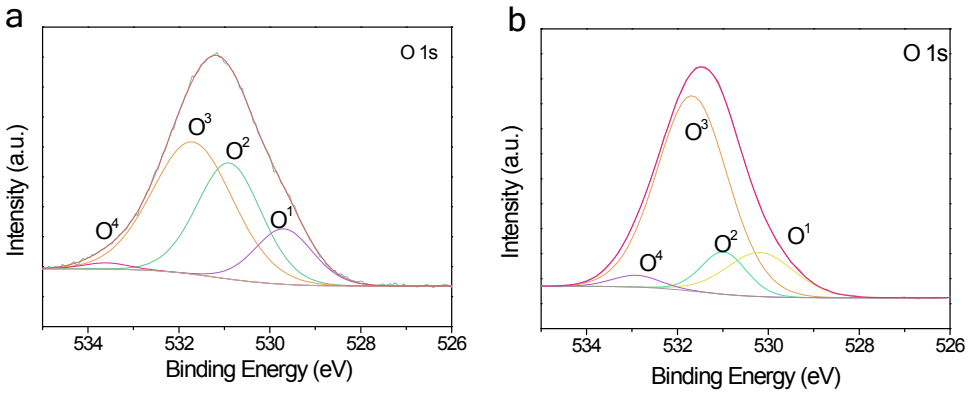

Figure S18. High resolution XPS spectrum of O 1s in (a) $(Ni_3Pt_7)_{0.5}$-$(MnO_x)_{0.5}$/ NPC-900 and (b) $(Ni_3Pt_7)_{0.5}$-$(MnO_x)_{0.5}$/NPC-900-2h.

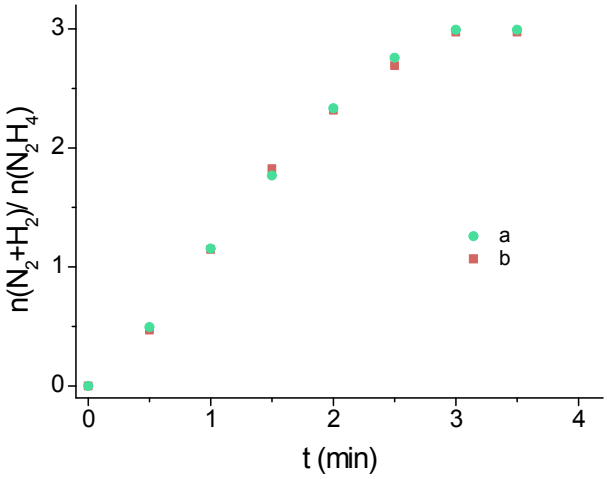

Figure S19. Catalytic performance tests of decomposition of hydrazine catalyzed by (a) $(Ni_3Pt_7)_{0.5}$-$(MnO_x)_{0.5}$/NPC-900, (b) $(Ni_3Pt_7)_{0.5}$ -$(MnO_x)_{0.5}$/NPC-900-2h.

Table S1. Pore characteristics of the obtained NPC samples and commercial carbon

Sample	BET surface area (m^2/g)	Pore volume (cm^3/g)	Pore Width (nm)
NPC-800	1322.8	1.083	1.18
NPC-900	1337.1	1.467	1.18
NPC-1000	1585.4	1.309	1.18

Table S2 Comparison of decomposition of hydrazine over different catalysts

Catalyst	T (K)	TOF (h^{-1})	Ea ($kJ \cdot mol^{-1}$)	Ref
$Pt_{0.6}Ni_{0.4}$/PDA-rGO	323	2056	33.39	1
$(Ni_3Pt_7)_{0.5}$-$(MnO_x)_{0.5}$ /NPC-900	323	706	50.15	This
$(Ni_3Pt_7)_{0.5}$-$(MnO_x)_{0.5}$ /NPC-900	303	210	50.15	work
Ni_3Pt_7/rGO	323	416	49.36	2
$Ni_{88}Pt_{12}$@MIL-101	323	371.5	51.29	3
Ni@Ni-Pt/La_2O_3	323	312	--	4
$Ni_{60}Pd_{40}$	298	30	--	5
$Ni_{30}Fe_{30}Pd_{40}$	318	21.5	40	6
$Rh_{0.8}Ni_{0.2}$@CeO_x/rGO	323	370	58	7
RhNiB	298	75	--	8
G4-OH($Pt_{12}Ni_{48}$)	343	225	--	9
$Rh_{4.4}Ni$/grapheme	298	13	--	10
Rh_2Ni nanooctahedra	293	47.1	41.6	11
$Ni_{40}Pt_{60}$-CNDs	323	594	43.9	12
$Rh_{55}Ni_{45}$/$Ce(OH)CO_3$	303	150	38.8	13
$Ni_{87}Pt_{13}$/MA	303	50		14
$CoIr_{0.081}$/ γ -Al_2O_3	298	28.7	--	15

Table S3. Percentages of different types of oxygen in $(Ni_3Pt_7)_{0.5}$-$(MnO_x)_{0.5}$/ NPC-900 and (b) $(Ni_3Pt_7)_{0.5}$-$(MnO_x)_{0.5}$/NPC-900-2h.

Element		$(Ni_3Pt_7)_{0.5}$-$(MnO_x)_{0.5}$/ NPC-900-0.5h	$(Ni_3Pt_7)_{0.5}$-$(MnO_x)_{0.5}$/ NPC-900-2h
O	Content of O Binding Energy (eV)	48.16%	68.28%
O^1 (%)	529.2 ± 0.2	14.77	15.5
O^2 (%)	530.8 ± 0.2	34.61	9.88
O^3 (%)	531.8 ± 0.2	49.32	71.7
O^4 (%)	533.0 ± 0.3	1.3	2.91

Possible attribution of O element

O^1 (%) : Metal-Oxygen Bonds (MnO, MnO_2, Mn_3O_4 and NiO)

O^2 (%) : Oxygen in -OH group

O^3 (%) : Oxygen bound in carbonate and/or bicarbonate groups

O^4 (%) : Physi-sorbed and chemi-sorbed water

Table S4. Pore characteristics of the obtained NPC samples and commercial carbon

Sample	BET surface area (m^2/g)	Pore volume (cm^3/g)	Pore Width (nm)
NPC-900	1337.1	1.467	1.18
$(Ni_3Pt_7)_{0.5}$-$(MnOx)_{0.5}$/NPC-900	147	0.2	1.23

Reference

1. F.-Z. Song, Q.-L. Zhu and Q. Xu, *J. Mater. Chem. A*, 2015, **3**, 23090-23094.
2. N. Cao, L. Yang, C. Du, J. Su, W. Luo and G. Cheng, *J. Mater. Chem. A*, 2014, **2**, 14344-14347.
3. N. Cao, L. Yang, H. Dai, T. Liu, J. Su, X. Wu, W. Luo and G. Cheng, *Inorg. Chem.*, 2014, **53**, 10122-10128.
4. Y.-J. Zhong, H.-B. Dai, Y.-Y. Jiang, D.-M. Chen, M. Zhu, L.-X. Sun and P. Wang, *J. Power Sources*, 2015, **300**, 294-300.
5. D. Bhattacharjee, K. Mandal and S. Dasgupta, *J. Power Sources*, 2015, **287**, 96-99.
6. D. Bhattacharjee and S. Dasgupta, *J. Mater. Chem. A*, 2015, **3**, 24371-24378.
7. Z. Zhang, Z.-H. Lu, H. Tan, X. Chen and Q. Yao, *J. Mater. Chem. A*, 2015, **3**, 23520-23529.
8. J. Wang, W. Li, Y. Wen, L. Gu and Y. Zhang, *Adv. Energy Mater.*, 2015, **5**.1401879.
9. K. Aranishi, A. K. Singh and Q. Xu, *ChemCatChem*, 2013, **5**, 2248-2252.
10. J. Wang, X.-B. Zhang, Z.-L. Wang, L.-M. Wang and Y. Zhang, *Energy Environ. Sci.*, 2012, **5**, 6885-6888.
11. C. Li, T. Wang, W. Chu, P. Wu and D. G. Tong, *Nanoscale*, 2016, DOI: 10.1039/C5NR09227B.
12. J.-K. Sun and Q. Xu, *ChemCatChem*, 2015, **7**, 526-531.
13. J. Chen, Q. Yao, J. Zhu, X. Chen and Z.-H. Lu, *Int. J. Hydrogen Energy*, 2016, **41**, 3946-3954.
14. Y. Jiang, Q. Kang, J. Zhang, H.-B. Dai and P. Wang, *J. Power Sources*, 2015, **273**, 554-560.
15. N. Firdous, N. K. Janjua, I. Qazi and M. H. Sarwar Wattoo, *Int. J. Hydrogen Energy*, 2016, **41**, 984-995.